

## COMPARATIVE ANALYSIS OF VARIABILITY IN THE MID-LATITUDE STRATOSPHERE AND IONOSPHERE IN WINTER PERIODS

**A.S. Yasyukevich**   
Institute of Solar-Terrestrial Physics SB RAS,  
Irkutsk, Russia, [anmpol@iszf.irk.ru](mailto:anmpol@iszf.irk.ru)

**A.M. Vesnin**   
Institute of Solar-Terrestrial Physics SB RAS,  
Irkutsk, Russia, [artem\\_vesnin@iszf.irk.ru](mailto:artem_vesnin@iszf.irk.ru)

**Abstract.** In this work, we perform a joint analysis of the spatial-temporal dynamics of ionospheric and stratospheric variability (with scales characteristic of internal gravity waves) at different longitudes of midlatitudes of the Northern Hemisphere. We analyze the winter periods of 2012–2013 and 2018–2019 when strong midwinter sudden stratospheric warmings (SSWs) occurred. An increase in the variability in the stratosphere is shown to occur in a limited latitude interval 40–60° N in the region of existence of a winter circumpolar vortex. Under SSW conditions, the generation of wave disturbances in the stratosphere ceases manifesting itself in a significant decrease in the stratospheric variability index. Similar behavior is noted in the spatial-temporal dynamics of the index of the total electron content vari-

ability. The level of ionospheric variability at midlatitudes decreases significantly after SSW peaks. The decrease in the ionospheric variability can be explained by a reduction in wave generation in the stratosphere, associated with the destruction of the circumpolar vortex during SSWs.

**Keywords:** ionosphere, total electron content, variability, internal gravity waves, stratosphere, circumpolar vortex, sudden stratospheric warmings, atmosphere-ionosphere interaction.

### INTRODUCTION

To date, it has been established that the degree of influence of sources in the underlying atmospheric layers on the state of ionospheric plasma may be quite high [Forbes et al., 2000]. One of the causes of the observed variations in the ionosphere is internal gravity waves (IGWs) propagating from the lower and middle atmosphere [Lastovicka, 2006] and realizing the dynamic relationship between different atmospheric layers [Yigit, Medvedev, 2016].

The circumpolar vortex (CPV) is a large-scale cyclonic-type circulation cell that forms in a cold air mass over the polar region in the upper stratosphere and the lower mesosphere in winter. Studies have revealed that CPV (and its associated jet stream) is a source of wave disturbances [Wu, Waters, 1996; Gerrard et al., 2011; Frisell et al., 2016; Liu et al., 2017]. Shpynev et al. [2015] have shown that inside CPV, conditions are created for the occurrence of baroclinic instabilities, which generate atmospheric waves of various scales, including IGW. Theoretical calculations estimated that IGW generation may take up to 10–15 % of the total energy of the jet stream [Shpynev et al., 2019].

IGWs generated above the stratopause are resistant to turbulent decay and can propagate upward at different angles over long distances [Kaifler et al., 2015], causing wave disturbances in the upper mesosphere, thermosphere, and hence in ionospheric plasma [Hocke, Schlegel, 1996]. Comparison of the wave variability in parameters of the neutral atmosphere and the ionosphere can provide information about the processes that determine the dynamic coupling between different atmospheric layers.

It has been established that in high and middle lati-

tudes the intensity of ionospheric wave disturbances with IGW periods has a pronounced seasonal dependence [Ratovsky et al., 2015; Frisell et al., 2016; Yasyukevich, 2021] with a maximum in the winter months. Frisell et al. [2016] and Yasyukevich et al. [2020c] have shown that there is a significant correlation between seasonal variations in the intensity of ionospheric disturbances and parameters of the neutral stratosphere in the CPV region. A possible connection between intensification of the winter ionospheric variability and the dynamics of the stratomesospheric jet stream over Eurasia was also observed in [Chernigovskaya et al., 2018].

The CPV and jet stream configuration varies greatly in winter, featuring significant spatial inhomogeneity; the strongest transformation of CPV occurs during periods of sudden stratospheric warmings (SSWs) [Labitzke, 1972; Schoeberl, 1978]. By SSW is meant a sudden, sharp increase in the temperature of the high-latitude stratosphere during the winter months, which is associated with an increase in wave activity [Matsuno, 1971; Charlton, Polvani, 2007]. The nonlinear interaction of planetary waves propagating from the troposphere with the normal stratospheric flow during SSW periods leads to a weakening or destruction of CPV in the high-latitude stratosphere. At the same time, the jet stream changes its position, and its shape is significantly modified. As a consequence, the IGW disturbances in the stratosphere are also generated unevenly.

In this study, we perform a joint analysis of the spatial-temporal dynamics of the intensity of IGW-scale wave disturbances in the ionosphere and stratosphere during the development and transformation of the circumpolar vortex in order to find a relationship between

disturbances in these atmospheric layers. For the analysis, we have taken the winters of 2012–2013 and 2018–2019, in the middle of which strong sudden stratospheric warmings were recorded.

## 1. DATA AND METHODS

We have used ECMWF ERA-5 Global reanalysis data to analyze the variability of the stratosphere and lower mesosphere in the Northern Hemisphere during the fall-winter periods. The archive provides data on the main atmospheric gas parameters acquired by assimilating measurements by ground-based and remote sensing methods in a global numerical model for forecasting the stratospheric and tropospheric conditions. The archive ensures high spatial resolution of the data (up to  $0.25^\circ$  or  $\sim 30$  km) in latitude and longitude up to a pressure level of 1 hPa (corresponds to an altitude of  $\sim 50$  km, the upper stratosphere — lower mesosphere level) [Hersbach et al., 2020]. In this work, we use data with a spatial resolution of  $0.75^\circ$  in latitude and longitude and a time resolution of 1 hr.

To estimate the variability level in the upper stratosphere — lower mesosphere, we propose a modified variability index  $stdW(\theta, \varphi, UT)$ , calculated from global fields of the vertical velocity of atmospheric gas  $W$ . The index at a given moment of universal time (UT) at each selected point with a given longitude  $\theta$  and latitude  $\varphi$  is defined as root mean square (RMS) of the vertical gas velocity  $W(\theta, \varphi, UT)$  at a given latitude from the mean value in a longitude range  $\theta \pm 10^\circ$ :

$$stdW(\theta, \varphi, UT) = \sqrt{\left( W(\theta, \varphi, UT) - \langle W(\theta \pm 10, \varphi, UT) \rangle \right)^2}. \quad (1)$$

The RMS calculation in such a longitude range excludes large-scale disturbances from consideration. It should be pointed out that the application of a fixed longitude boundary will lead to a difference in the lower boundary of filtered variations at different latitudes. Since dealing with a limited latitude interval ( $40^\circ$ – $60^\circ$  N), we exclude variations with a wavelength over 1700–2500 km from the consideration. Estimates of typical scales of disturbances observed in vertical velocity distributions in the CPV region, given in [Shpynev et al., 2016], have shown that the spectrum of the disturbances is maximum at wavelengths 300–1000 km (this scale corresponds to IGW). Thus, applying a filter with the given boundaries makes it possible to take into account the most intense variations when calculating the index; and the variability index we propose reflects the intensity of wave disturbances with scales characteristic of IGW. The index is measured in the same values as the vertical velocity  $W$  [cPa/s].

A similar index was exploited in [Yasyukevich et al., 2020c] to estimate seasonal variations in the stratospheric variability along the given latitude. However, the RMS calculation was made along the entire zonal circle, which did not allow us to estimate spatial variations in such an index.

To analyze the short-period ionospheric variability, we used vertical total electron content (TEC) data ob-

tained from measurements at a worldwide network of GNSS signal receivers, processed and provided by the OpenMadrigral database Center [Rideout, Coster, 2006]. The initial data has a spatial resolution of  $1^\circ \times 1^\circ$  in latitude and longitude and a time step of 5 min.

For the calculations, all initial TEC data was sorted into  $3^\circ \times 3^\circ$  cells in latitude and longitude around the globe. The TEC value in each grid cell was obtained by averaging all the initial TEC values fell into the cell. This approach is necessary to increase the amount of data because a specific cell of the original grid is not always filled with TEC value due to motion of satellites. If tolerance to omissions was zero, the volume of filled cells would not allow research to be conducted over a long period of time. Moreover, in regions with a small number of stations, Madrigal TEC data may be characterized by errors and frequent absence of data in individual cells [Yasyukevich et al., 2020a]. Therefore, for ionospheric research in regions with a small number of receiving stations it is possible to adopt other services such as SI-MuRG — System for Ionosphere Monitoring and Research from GNSS [Yasyukevich et al., 2020b]. In regions with a dense network of stations, the quality of Madrigal data is as high as that of other services [Rideout, Coster, 2006]. In view of the foregoing, we have selected two longitudes in the North American ( $240^\circ$  E) and European ( $10^\circ$  E) sectors, at which the density of stations (and hence TEC data) in the Northern Hemisphere is high in both periods of interest.

The short-period variability index  $vrTEC(UT)$  was calculated in each grid cell [Yasyukevich et al., 2017]. For the moment of time UT, the index is derived by calculating RMS of TEC ( $TEC$ ) at a given interval, centered on the middle of this interval and normalized to mean TEC in this window:

$$vrTEC(UT) = \frac{\sqrt{\left( TEC(UT) - \langle TEC(UT \pm 2) \rangle \right)^2}}{\langle TEC(UT \pm 2) \rangle}, \quad (2)$$

where  $\langle TEC(UT \pm 2) \rangle$  is TEC averaging over a given time interval. For the index to reflect the level of variability with IGW scales, the averaging interval should be limited to several hours (in this paper, 4 hrs). The index is a dimensionless value showing the intensity of TEC fluctuations within a given interval relative to the mean TEC value. The normalization allows us to compare the nighttime and daytime TEC variability. Note that the time resolution of the initial TEC data does not allow us to estimate the contribution of the smallest-scale acoustic disturbances (with periods less than 10 min); therefore, the short-period variability index used in the work incorporates TEC variations with periods from  $\sim 10$  min to  $\sim 4$  hrs. Such periods are typical of IGW. This index has been employed in [Yasyukevich et al., 2020c] to analyze seasonal variations in short-period ionospheric variability. Examples of the  $vrTEC(UT)$  index distributions obtained in the Northern Hemisphere at latitudes  $15$ – $90^\circ$  N for December 19, 2018 and January 13, 2019 at 0 UT are given in Figure 1.

The resulting  $vrTEC(UT)$  values were used to plot time-latitude distributions of the ionospheric variability at the given longitudes. Yasyukevich [2021] has indicated

that the short-period TEC variability experiences significant intradiurnal variations. At a mid-latitude station, two distinct peaks are distinguished in the diurnal variability near the time of passage of solar terminators, which are the source of ionospheric disturbances of various scales [Afraimovich et al., 2009]. At a high-latitude station, the variability increases significantly at night. This may be due to auroral activity that intensifies at night. In order to exclude the influence of these disturbing factors when obtaining latitude-time distributions of ionospheric disturbances at each latitude, we averaged all  $vrTEC(UT)$  values corresponding only to near-noon local time (10–14 LT) at a given longitude. Time averaging is necessary for correct comparison with the dynamics of the  $stdW(\theta, \varphi, UT)$  index whose time resolution is significantly lower. To obtain the time-latitude distributions of the stratospheric variability index, we take  $stdW(\theta, \varphi, UT)$  at the moment of UT closest to the local noon at the longitude under study. Thus, we compare the dynamics of distributions of the ionospheric and stratospheric variability for the local daytime.

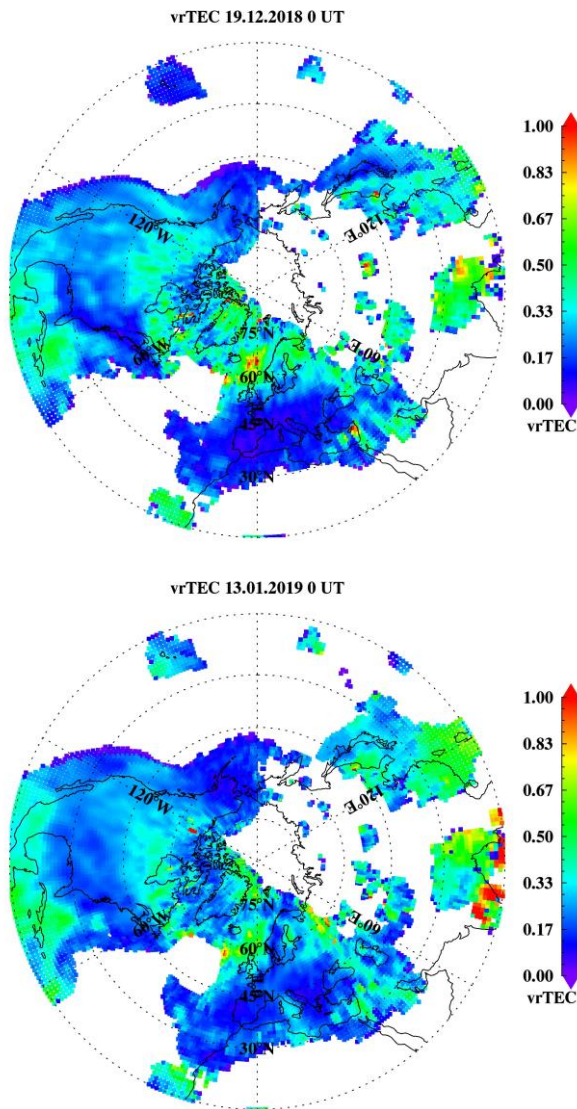


Figure 1. Distributions of the ionospheric variability index  $vrTEC(UT)$  on December 19, 2018 (top) and January 13, 2019 (bottom) at 0 UT (Northern Hemisphere, polar view)

## 2. SHORT-PERIOD VARIABILITY IN THE STRATOSPHERE AND IONOSPHERE

Figure 2 exemplifies distributions of fields of horizontal wind (a), vertical velocity of atmospheric gas  $W$  (b),

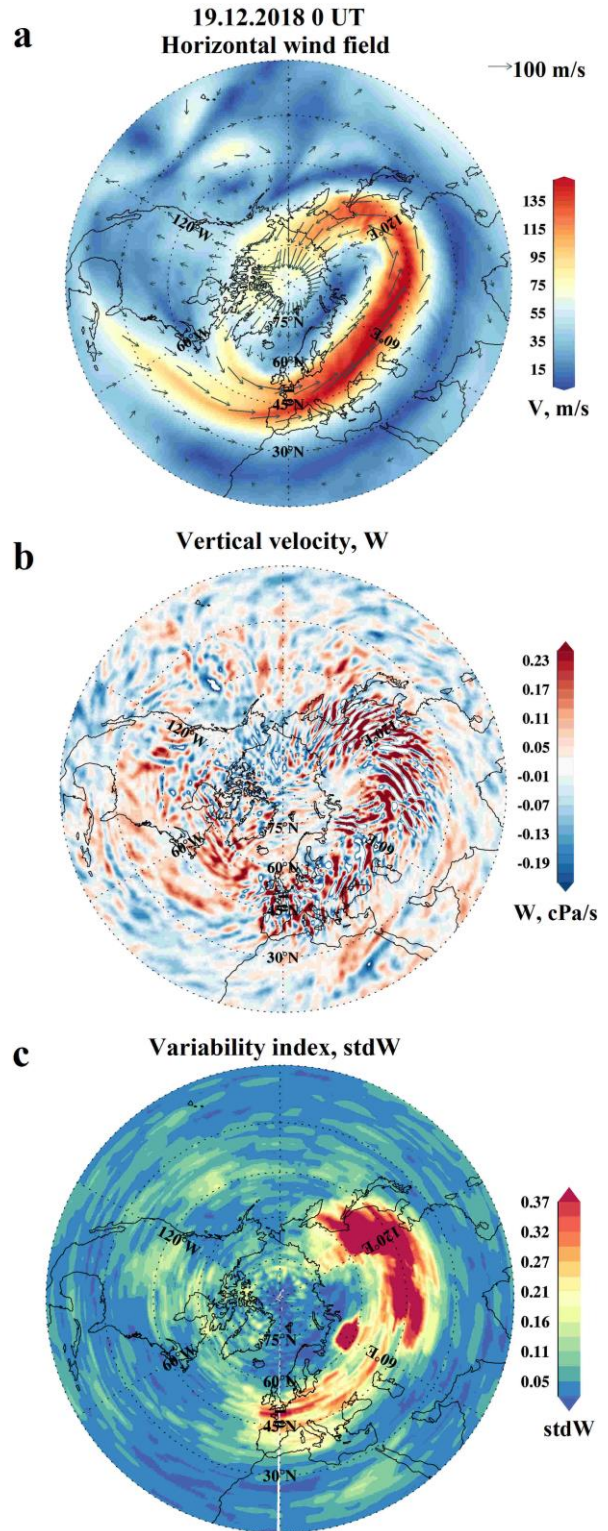


Figure 2. Distribution of fields of horizontal wind (a), vertical velocity of atmospheric gas  $W$  (b), and variability index  $stdW(\theta, \varphi, UT)$  (c) at the level of 1 hPa on December 19, 2018 (Northern Hemisphere, polar view)

and  $stdW(\theta, \varphi, UT)$  ( $c$ ) at the level of 1 hPa (about 50 km) on December 19, 2018 (polar view). There is a well-developed jet stream rounding the Pole. The jet stream is accompanied by pronounced medium-scale wave disturbances, clearly observed in variations of the vertical velocity at latitudes  $40^\circ$ – $60^\circ$  N. The variability index distribution suggests that the greatest intensity of disturbances is recorded in regions with high horizontal wind velocity gradients in the jet stream:  $\sim 40^\circ$ – $60^\circ$  N and  $\sim 60^\circ$ – $150^\circ$  E.

Figure 3 demonstrates similar distributions for January 13, 2019 — the period after the peak of strong SSW.

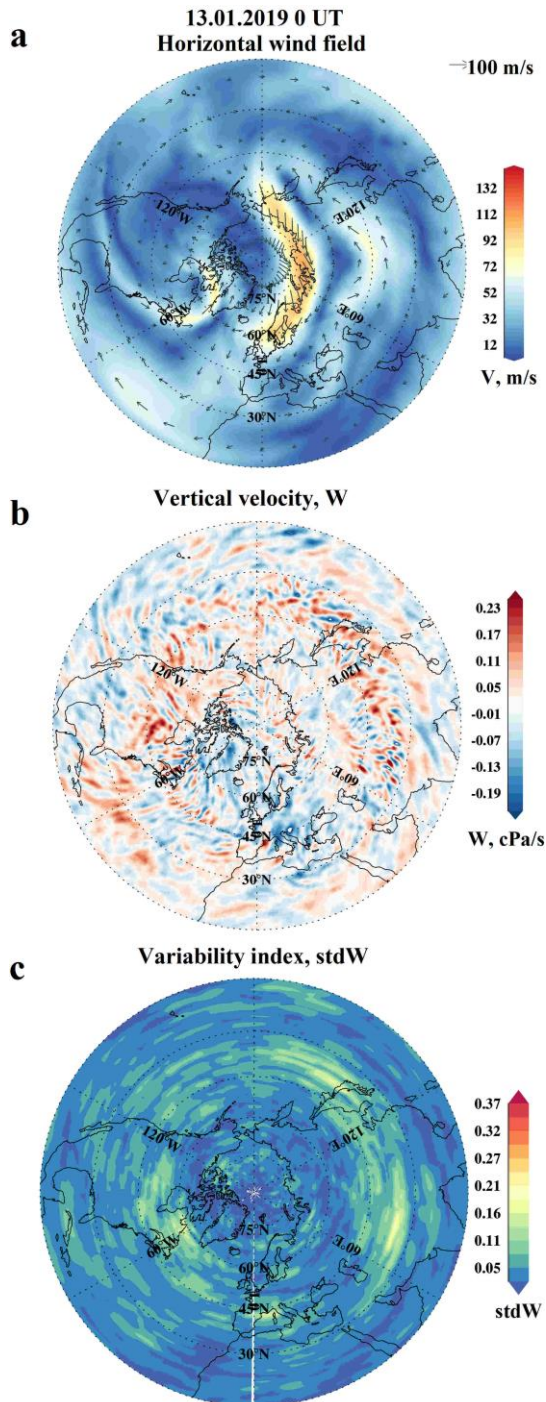


Figure 3. Distributions of fields of horizontal wind ( $a$ ), vertical atmospheric gas velocity  $W$  ( $b$ ), and variability index  $stdW(\theta, \varphi, UT)$  ( $c$ ) at the level of 1 hPa on January 13, 2019 (Northern Hemisphere, polar view)

We can see that the CPV structure has been significantly changed and there is no jet stream in near-polar latitudes. At the same time, there is a significant weakening of wave disturbances, which is reflected in the low stratospheric variability index. Thus, after strong SSW the source of generation of small-scale disturbances in the stratosphere is "turned off", which may affect the variability of higher atmospheric layers.

Figures 4, 5 show latitude-time distributions of indices of variability in TEC (left) and in the upper stratosphere at the level of 1 hPa (right) at two longitudes in the European (top) and American (bottom) sectors during the winter periods 2012–2013 and 2018–2019 respectively. We have considered the latitude range  $40^\circ$ – $60^\circ$  N, where the intensity of stratospheric disturbances in the CPV region is maximum (see Figure 2,  $c$ ). The winter periods of interest are marked by the occurrence of strong SSW in the stratosphere. Peak dates for the SSW events (the day of the mean circulation reversal at the level of 10 hPa) were respectively January 6, 2013 and January 1, 2019.

The above Figures show that the stratospheric variability features a significant space-time inhomogeneity. The level of variability in both winter periods is significantly higher in the European sector than in the American one (the intensity of the color scale differs twice). In the first winter month when there is a well-developed CPV and a stable jet stream in the stratosphere, the variability is high, indicating the continuous generation of wave disturbances in the jet stream region.

During strong SSW, the circumpolar vortex and its related jet stream first shift to the Pole, and then break down. During both winter periods after the SSW peaks, the stratospheric variability decreases significantly. The low variability level persists for about a month. Then CPV recovers and the intensity of disturbances increases.

Similar variations can be found in the time-latitude distributions of the ionospheric variability index. Thus, an increase in the variability level occurs at the beginning of the winter periods considered. After SSW peaks (in mid-January), the variability level in the ionosphere decreases considerably.

Note that the intensity of disturbances in the ionosphere changes with a delay relative to similar variations in the stratosphere ( $\sim 7$ – $10$  days). For example, a sharp increase in the intensity of disturbances at latitudes  $50^\circ$ – $60^\circ$  N in the North American sector is recorded in the stratosphere on January 5–10, 2013 (Figure 4,  $d$ ) and January 10–15, 2013 in TEC (Figure 4,  $c$ ). This agrees with the results reported by Yasyukevich et al. [2020c]; the authors have shown that the cross-correlation function between stratospheric and ionospheric variations was maximum at mid-latitude stations with a delay from  $\sim 10$  to 20 days. Tolstikov et al. [2021] have carried out a comprehensive study of manifestations of wave activity with IGW periods in different regions of the atmosphere: the stratosphere, the upper mesosphere, and the F2-region of the ionosphere. The authors have demonstrated that the best correlation between stratospheric activity and IGW variability in the ionosphere is observed when stratospheric activity is delayed by  $\sim 15$  days. According to the authors, the  $\sim 15$  day

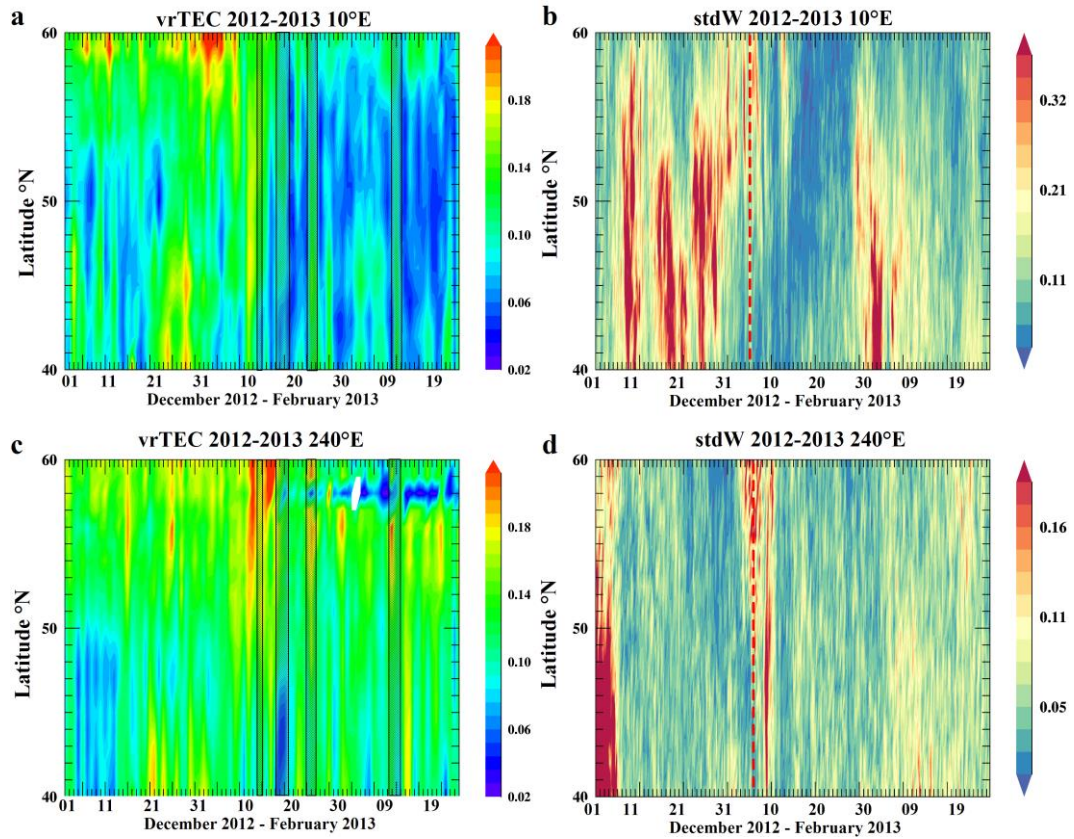


Figure 4. Latitude-time distributions of variability indices in the ionosphere (left) and in the upper stratosphere (right) at two longitudes in the European (top) and American (bottom) sectors in the winter of 2012–2013. Periods of geomagnetic disturbances on panels *a* and *c* are marked with a gray fill. Red dashes on panels *b*, *d* indicate peak dates of SSW

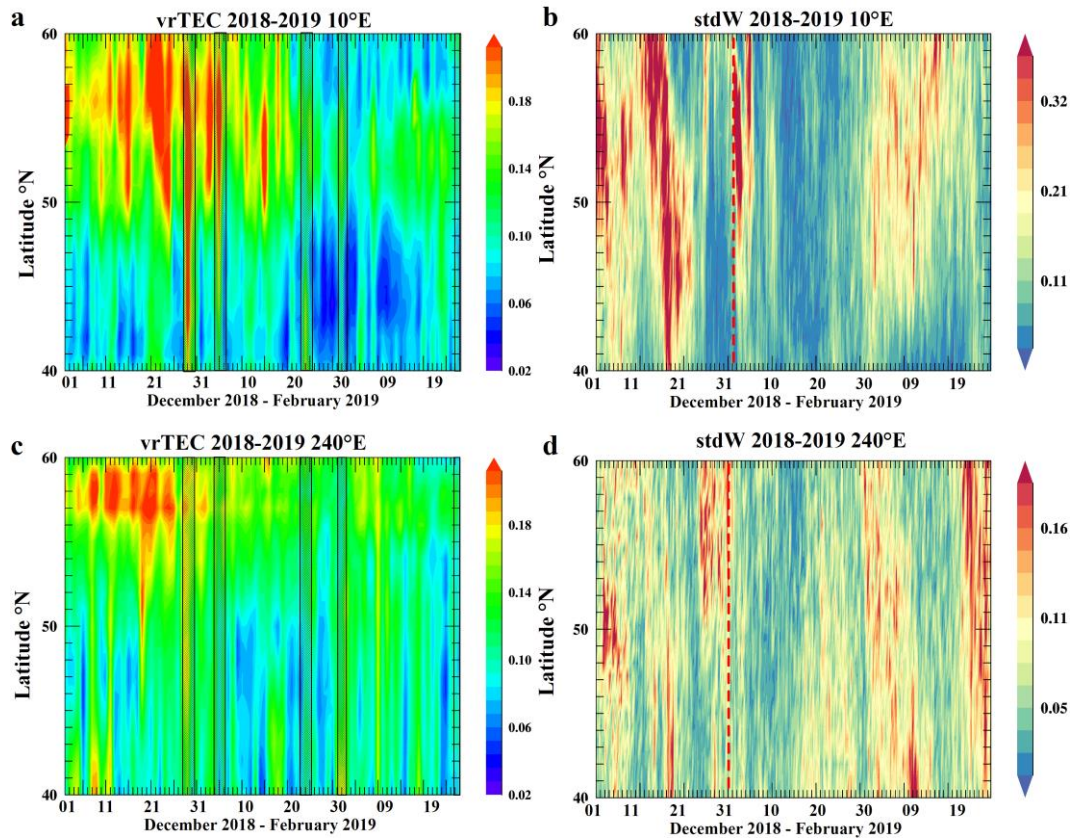


Figure 5. Latitude-time distributions of variability indices in the ionosphere (left) and in the upper stratosphere (right) at two longitudes in the European (top) and American (bottom) sectors in the winter of 2018–2019. Periods of geomagnetic disturbances on panels *a* and *c* are marked with a gray fill. Red dashes on panels *b*, *d* indicate peak dates of SSW

delay between the IGW variability and stratospheric activity can be explained by the corresponding delay in temperature variations at heights of the lower thermosphere relative to temperature variations in the stratosphere. Thus, our findings are consistent with the previously published ones.

Note also the presence in the distribution of the ionospheric variability of periodic structures with longer periods (~5–6 days), most pronounced in 2018–2019 (Figure 5, *a, c*). These variations may be associated with the impact of planetary waves whose intensity also increases significantly during an SSW [Pancheva et al., 2008]. Planetary waves can propagate upward, affecting the mesosphere — lower thermosphere parameters [Zorkaltseva, Vasiliev, 2021], and modulate the IGW amplitude through the wave-wave interaction mechanism. The study of such large-scale disturbances is, however, beyond the scope of this work.

When comparing the variability in the stratosphere and ionosphere, we should take into account the fact that the ionospheric variability, along with the effects of underlying atmospheric layers, depends on a large number of factors, such as solar and geomagnetic activity, regular disturbances in the auroral oval (at high latitudes), etc. It cannot, therefore, be expected that the latitude-time pattern of the ionospheric variability will strictly repeat such a pattern in the stratosphere.

The dynamics of solar and geomagnetic activity indices according to the OmniWeb service [<https://omniweb.gsfc.nasa.gov/form/dx1.html>] is shown in Figure 6. Note that in general the helio-geomagnetic conditions during the periods of interest were fairly quiet. There were isolated periods of weak geomagnetic disturbances ( $K_p \leq 4.3$ ). The most intense geomagnetic disturbances ( $K_p \leq 5.3$ ) were recorded on January 4–5 and January 31 – February 2, 2019. All the periods with  $K_p$  exceeding 3.5 are marked in Figures 4 and 5 with a gray fill. In the variations of the ionospheric variability index, we can identify intensifications associated with changes in geomagnetic conditions. At the same time, the geomagnetic variations cannot explain most of the variations in the ionospheric variability index observed during the periods considered. The most significant changes in solar activity occurred on January 2013: the  $F 10.7$  index increased sharply from ~100 to ~170 s.f.u. (Figure 6, *a*), yet there are no similar variations in the dynamics of the ionospheric variability index.

Thus, the synchronous decrease observed in the level of variability in the stratosphere and ionosphere after the peaks of strong SSW indicates a connection between variability in these atmospheric layers and is evidence of the impact of wave disturbances occurring in the CPV region at stratospheric heights on ionospheric plasma. A similar decrease in IGW activity in the ionosphere after the peak of strong SSW in the winter 2008–2009 has been detected by Nayak, Yiğit [2019]. The authors suggested that the decrease in IGW activity is related to changes in wave propagation conditions. Nonetheless, our findings suggest that the main cause may be the destruction of CPV and, as a consequence, cessation of generation of waves in the stratosphere.

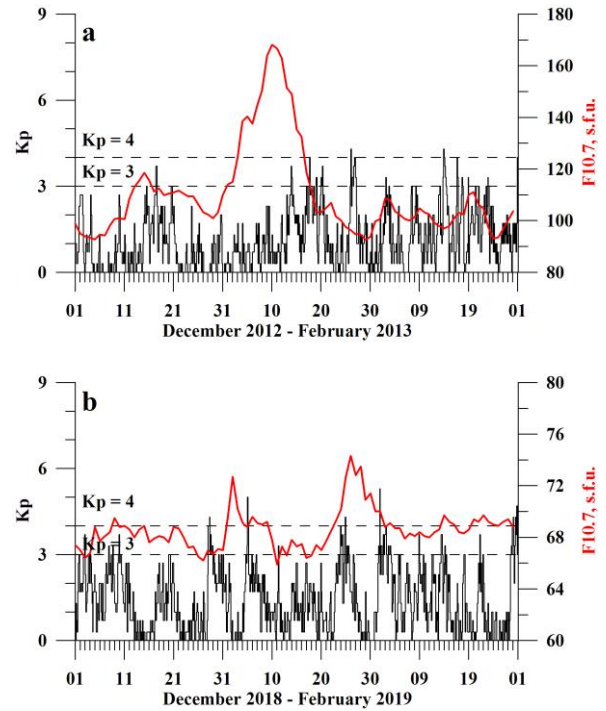


Figure 6. Dynamics of geomagnetic activity indices ( $K_p$ , black curves) and solar radio emission flux ( $F10.7$ , red curves) during periods of interest

## CONCLUSION

We have carried out a joint analysis of the spatio-temporal dynamics of variability (with IGW scales) in the ionosphere and stratosphere during the winter periods 2012–2013 and 2018–2019 at midlatitudes and two longitudes in the European and North American sectors. These periods featured the occurrence of strong sudden stratospheric warmings when a significant transformation of the circumpolar vortex and its associated jet stream occurred in the stratosphere.

The stratospheric variability is shown to exhibit a significant space-time inhomogeneity. The maximum stratospheric variability index is recorded in the regions characterized by high gradients of horizontal wind velocity in the jet stream. During both winter periods considered, after SSW peaks there is a significant decrease in the stratospheric variability, observed for about a month.

Similar variations have been found in the latitude-time distributions of the ionospheric variability index at midlatitudes: an increase in the variability level at the beginning of the winters considered and a significant decrease in the variability in mid-January after the SSW peaks.

Cessation of generation of wave disturbances in the stratosphere, associated with the destruction of the circumpolar vortex and jet stream during the SSW periods, may explain the decrease in the ionospheric variability in the middle of the winter periods studied.

We are grateful to MIT Haystack Observatory for Madrigal TEC data, to ECMWF for ERA5 Reanalysis archive data, as well as to OmniWeb service for data on helio-geomagnetic activity indices. The work was financially supported by RSF (Grant No. 20-77-00070).

## REFERENCES

- Afraimovich E.L., Edemskiy I.K., Voeykov S.V., Yasyukevich Yu.V., Zhivetiev I.V. The first GPS-TEC imaging of the space structure of MS wave packets excited by the solar terminator. *Ann. Geophys.* 2009, vol. 27, pp. 1521–1525. DOI: [10.5194/angeo-27-1521-2009](https://doi.org/10.5194/angeo-27-1521-2009).
- Charlton A.J., Polvani L.M. A new look at stratospheric sudden warmings. Part I: climatology and modeling benchmarks. *J. Climate.* 2007, vol. 20, pp. 449–469. DOI: [10.1175/JCLI3996.1](https://doi.org/10.1175/JCLI3996.1).
- Chernigovskaya M.A., Shpynev B.G., Ratovsky K.G., Belinskaya A.Yu., Stepanov A.E., Bychkov V.V., Grigorieva S.A., Panchenko V.A., Korenkova N.A., Mielich J. Ionospheric response to winter stratosphere/lower mesosphere jet stream in the Northern Hemisphere as derived from vertical radio sounding data. *J. Atmos. Solar-Terr. Phys.* 2018, vol. 180, pp. 126–136. DOI: [10.1016/j.jastp.2017.08.033](https://doi.org/10.1016/j.jastp.2017.08.033).
- Forbes J.M., Palo S.E., Zhang X. Variability of the ionosphere. *J. Atmos. Solar-Terr. Phys.* 2000, vol. 62, iss. 8, pp. 685–693. DOI: [10.1016/S1364-6826\(00\)00029-8](https://doi.org/10.1016/S1364-6826(00)00029-8).
- Frissell N.A., Baker J.B.H., Ruohoniemi J.M., Greenwald R.A., Gerrard A.J., Miller E.S., West M.L. Sources and characteristics of medium-scale traveling ionospheric disturbances observed by high-frequency radars in the North American sector. *J. Geophys. Res.* 2016, vol. 121, pp. 3722–3739. DOI: [10.1002/2015JA022168](https://doi.org/10.1002/2015JA022168).
- Gerrard A.J., Bhattacharya Y., Thayer J.P. Observations of in-situ generated gravity waves during a stratospheric temperature enhancement (STE) event. *Atmos. Chemistry Phys.* 2011, vol. 11, pp. 11913–11917. DOI: [10.5194/acp-11-11913-2011](https://doi.org/10.5194/acp-11-11913-2011).
- Hersbach H., Bell B., Berrisford P., Hirahara S., Horányi A., Muñoz-Sabater J., Nicolas J., Peubey C., Radu R., et al. The ERA5 global reanalysis. *Quarterly Journal of the Royal Meteorological Society.* 2020, vol. 146, pp. 1999–2049. DOI: [10.1002/qj.3803](https://doi.org/10.1002/qj.3803).
- Hocke K., Schlegel K. A review of atmospheric gravity waves and travelling ionospheric disturbances: 1982–1995. *Ann. Geophys.* 1996, vol. 14, pp. 917–940. DOI: [10.1007/s00585-996-0917-6](https://doi.org/10.1007/s00585-996-0917-6).
- Kaifler B., Lübken F.-J., Höffner J., Morris R.J., Viehl T.P. Lidar observations of gravity wave activity in the middle atmosphere over Davis (69° S, 78° E), Antarctica. *J. Geophys. Res. Atmos.* 2015, vol. 120, pp. 4506–4521. DOI: [10.1002/2014JD022879](https://doi.org/10.1002/2014JD022879).
- Labitzke K. Temperature changes in the mesosphere and stratosphere connected with circulation changes in winter. *J. Atmos. Sci.* 1972, vol. 29, pp. 756–766. DOI: [10.1175/1520-0469\(1972\)029<0756:TCITMA>2.0.CO;2](https://doi.org/10.1175/1520-0469(1972)029<0756:TCITMA>2.0.CO;2).
- Lastovicka J. Forcing of the ionosphere by waves from below. *J. Atmos. Solar-Terr. Phys.* 2006, vol. 68, pp. 479–497. DOI: [10.1016/j.jastp.2005.01.018](https://doi.org/10.1016/j.jastp.2005.01.018).
- Liu X., Yue J., Xu J., Garcia R.R., Russell III, J.M., Mlynczak M., Wu D.L., Nakamura T. Variations of global gravity waves derived from 14 years of SABER temperature observations. *J. Geophys. Res. Atmos.* 2017, vol. 122, pp. 6231–6249. DOI: [10.1002/2017JD026604](https://doi.org/10.1002/2017JD026604).
- Matsuno T. A dynamical model of the stratospheric sudden warming. *J. Atmos. Sci.* 1971, vol. 28, pp. 1479–1494. DOI: [10.1175/1520-0469\(1971\)028<1479:ADMOTS>2.0.CO;2](https://doi.org/10.1175/1520-0469(1971)028<1479:ADMOTS>2.0.CO;2).
- Nayak C., Yiğit E. Variation of small-scale gravity wave activity in the ionosphere during the major sudden stratospheric warming event of 2009. *J. Geophys. Res.: Space Phys.* 2019, vol. 124, pp. 470–488. DOI: [10.1029/2018JA026048](https://doi.org/10.1029/2018JA026048).
- Pancheva D., Mukhtarov P., Mitchell N.J., Merzlyakov E., Smith A.K., Andonov B., Singer W., Hocking W., Meek C., Manson A., Murayama Y. Planetary waves in coupling the stratosphere and mesosphere during the major stratospheric warming in 2003/2004. *J. Geophys. Res.* 2008, vol. 113, D12105. DOI: [10.1029/2007JD009011](https://doi.org/10.1029/2007JD009011).
- Ratovsky K.G., Medvedev A.V., Tolstikov M.V. Diurnal, seasonal and solar activity pattern of ionospheric variability from Irkutsk Digisonde data. *Adv. Space Res.* 2015, vol. 55, pp. 2041–2047. DOI: [10.1016/j.asr.2014.08.001](https://doi.org/10.1016/j.asr.2014.08.001).
- Rideout W., Coster A. Automated GPS processing for global total electron content data. *GPS Solutions.* 2006, vol. 10, pp. 219–228. DOI: [10.1007/s10291-006-0029-5](https://doi.org/10.1007/s10291-006-0029-5).
- Schoeberl M.R. Stratospheric warmings: observations and theory. *J. Geophys. Res.: Space Phys.* 1978, vol. 16, pp. 521–538. DOI: [10.1029/RG016i004p00521](https://doi.org/10.1029/RG016i004p00521).
- Shpynev B.G., Churilov S.M., Chernigovskaya M.A. Generation of waves by jet-stream instabilities in winter polar stratosphere/mesosphere. *J. Atmos. Solar-Terr. Phys.* 2015, vol. 136(B), pp. 201–215. DOI: [10.1016/j.jastp.2015.07.005](https://doi.org/10.1016/j.jastp.2015.07.005).
- Shpynev B.G., Chernigovskaya M.A., Khabituev D.S. Spectral characteristics of atmospheric waves generated by winter stratospheric jet stream in the Northern Hemisphere. *Sovremennye problemy distantsionnogo zondirovaniya Zemli iz kosmosa.* 2016, vol. 13, iss. 2, pp. 120–131. DOI: [10.21046/2070-7401-2016-13-2-120-131](https://doi.org/10.21046/2070-7401-2016-13-2-120-131). (In Russian).
- Shpynev B.G., Khabituev D.S., Chernigovskaya M.A., Zorkal'tseva O.S. Role of winter jet stream in the middle atmosphere energy balance. *J. Atmos. Solar-Terr. Phys.* 2019, vol. 188, pp. 1–10. DOI: [10.1016/j.jastp.2019.03.008](https://doi.org/10.1016/j.jastp.2019.03.008).
- Tolstikov M.V., Ratovsky K.G., Medvedeva I.V., Khabituev D.S. Estimated influence of stratospheric activity on the ionosphere according to measurements with ISTP SB RAS tools. *Solar-Terr. Phys.* 2021, vol. 7, iss. 4, pp. 79–84. DOI: [10.12737/stp-74202108](https://doi.org/10.12737/stp-74202108).
- Wu D.L., Waters J.W. Satellite observations of atmospheric variances: A possible indication of gravity waves. *Geophys. Res. Lett.* 1996, vol. 23, iss. 24, pp. 3631–3634. DOI: [10.1029/96GL02907](https://doi.org/10.1029/96GL02907).
- Yasyukevich A.S. Features of short-period variability of total electron content at high and middle latitudes. *Solar-Terr. Phys.* 2021, Vol. 7, iss. 4, P. 71–78. DOI: [10.12737/stp-74202107](https://doi.org/10.12737/stp-74202107).
- Yasyukevich A.S., Chernigovskaya M.A., Mylnikova A.A., Shpynev B.G., Khabituev D.S. Studying the seasonal pattern of the ionospheric variability over Eastern Siberia and Far East region from the GPS/GLONASS data. *Sovremennye problemy distantsionnogo zondirovaniya Zemli iz kosmosa.* 2017, vol. 14, iss. 3, pp. 249–262. DOI: [10.21046/2070-7401-2017-14-4-249-262](https://doi.org/10.21046/2070-7401-2017-14-4-249-262). (In Russian).
- Yasyukevich Yu., Mylnikova A., Vesnin A. GNSS-Based Non-Negative Absolute Ionosphere Total Electron Content, its Spatial Gradients, Time Derivatives and Differential Code Biases: Bounded-Variable Least-Squares and Taylor Series. *Sensors.* 2020a, vol. 20, iss. 19, 5702. DOI: [10.3390/s20195702](https://doi.org/10.3390/s20195702).
- Yasyukevich Y.V., Kiselev A.V., Zhivetiev I.V., Edemskiy I.K., Syrovatskii S.V., Maletckii B.M., Vesnin A.M. SIMuRG: System for Ionosphere Monitoring and Research from GNSS. *GPS Solut.* 2020b, vol. 24, 69. DOI: [10.1007/s10291-020-00983-2](https://doi.org/10.1007/s10291-020-00983-2).
- Yasyukevich A., Medvedeva I., Sivtseva V., Chernigovskaya M., Ammosov P., Gavriilyeva G. Strong interrelation between the short-term variability in the ionosphere, upper mesosphere, and winter polar stratosphere. *Remote Sens.* 2020c, vol. 12, 1588. DOI: [10.3390/rs12101588](https://doi.org/10.3390/rs12101588).
- Yiğit E., Medvedev A.S. Role of gravity waves in vertical coupling during sudden stratospheric warmings. *Geosci. Lett.* 2016, vol. 3, 27. DOI: [10.1186/s40562-016-0056-1](https://doi.org/10.1186/s40562-016-0056-1).
- Zorkal'tseva O.S., Vasilyev R.V. Stratospheric influence on the mesosphere–lower thermosphere over mid latitudes in

winter observed by a Fabry–Perot interferometer. *Ann. Geophys.* 2021, vol. 39, pp. 267–276. DOI: [10.5194/angeo-39-267-2021](https://doi.org/10.5194/angeo-39-267-2021).

URL: <https://omniweb.gsfc.nasa.gov/form/dx1.html> (accessed March 30, 2022).

Original Russian version: Yasyukevich A.S., Vesnin A.M., published in *Solnechno-zemnaya fizika*. 2022. Vol. 8. Iss. 2. P. 67–74. DOI: [10.12737/szf-82202209](https://doi.org/10.12737/szf-82202209). © 2022 INFRA-M Academic Publishing House (Nauchno-Izdatelskii Tsentr INFRA-M)

*How to cite this article*

Yasyukevich A.S., Vesnin A.M. Comparative analysis of variability in the mid-latitude stratosphere and ionosphere in winter periods. *Solar-Terrestrial Physics*. 2022. Vol. 8. Iss. 2. P. 61–68. DOI: [10.12737/stp-82202209](https://doi.org/10.12737/stp-82202209).